Finite Element Analysis to Predict The Effect of Basalt Macro Fibers on the Shear Strength and Behavior of BFRP-Reinforced Concrete Beams

By:
Jaza Hassan Muhammad

March - 2024

1.1 Finite Element Modeling Background

In recent years, finite element analysis (FEA) has developed into a potentially more useful tool for study and design. Under the condition that the user possesses adequate modeling knowledge, a comprehensive analysis can become a useful entity for various engineering applications. During modeling, utilizing the wrong approach or aspect might result in the wrong answer. So, experimental results or a closed-form solution must be provided to validate the results of any FEA and have complete trust in them. The fundamental benefit of FEA is its capacity to recreate pricey tests and offer simple solutions to complex problems. By utilizing various element types, different properties of materials, and multiple loading and boundary conditions, the FEA may be used for various engineering applications.

This study simulated the shear strength and behavior of BFRP-reinforced concrete beams reinforced with basalt macro fiber (BFRP-BMF-RC beams) with and without stirrups using the FEA program ABAQUS 2019. Due to its large library of materials and elements, capacity to simulate multi-dimensional problems, and popularity in academic and research organizations, ABAQUS is a popular finite element analysis (FEA) program. Eighteen BFRP-RC beams without stirrups were modeled, considering the effect of Basalt Macro fibers (BMF), concrete compressive, and the BFRP reinforcement ratio. In addition, three BFRP-RC beams with stirrups were modeled considering the stirrup contribution

1.1.1 Meshing and Defining Element Types

The concrete was modeled with an 8-node linear brick solid element, reduced integration, and hourglass control (C3D8R). This element provides an acceptable solution to the most three-dimensional model. Each 3D continuum element has eight nodes, each node having 3 degrees of freedom. This type of element has only one integration point (Gauss point) located at the centroid of the elements. It can be used in Abaqus/Explicit and Abaqus/Standard for linear and nonlinear analysis. Abaqus adds a small amount of artificial "hourglass stiffness" to linear reduced integration

elements to limit the model's hourglass propagation. Reasonably fine mesh used to first-order reduced integration elements leads to more acceptable results [1]. The mesh size was calibrated to 10 mm in this study. A 2-node linear 3D truss element (T3D2) representing the longitudinal and transverse BFRP bars was used. Each node of the truss element has 3 degrees of freedom. The steel plates 20 x 60 x 150 mm were used for supports and loading points to prevent stress concentration problems and distribute the loads equally on the loaded area. The C3D8R element type was also used to model these plates and distribute the loads equally in the loaded area.

1.1.2 Concrete Constitutive Models

To represent the nonlinear behavior of concrete, ABAQUS includes three material models: brittle cracking, concrete smeared cracking, and the Concrete Damaged Plasticity Model (CDPM). The CDPM, which explains the inelastic behavior of concrete using the principles of isotropic damaged elasticity combined with isotropic tensile and compressive plasticity, could be regarded as one of the best models for modeling complex concrete behavior. The CDPM established by Lubliner et al. [2] and developed by Lee and Fevnes [3] is based on the plasticity theory for the nonlinear analysis of brittle materials. The model considers the degradation of elastic stiffness induced by plastic straining in tension and compression. [1].

1.1.2.1 Uniaxial tension stress behavior and defining tension stiffening

The stress-strain behavior under uniaxial tension is a linear elastic relationship $\sigma_t = E_0 \varepsilon_t$ until the cracking stress (σ_{cr}). This study used the splitting tensile strength to evaluate the cracking stress. Therefore, to obtain cracking stress of concrete from splitting tensile strength $0.7 f_{sp}$ was used, as Kim and Taha [4] recommended. The stress-strain softening response rather than hardening is observed beyond the cracking stress if the fiber volume fraction is less than 2% [5]. In the post-cracking region of reinforced concrete, tension stiffening occurs, allowing the strain-softening of cracked concrete to be defined. This behavior also simulates the effects of

reinforcing interaction with concrete [6]. Moreover, tension stiffening significantly affects the modeling of fiber-reinforced concrete beams. Eq. (1) is the simple expression suggested by Okamura and Maekawa [7] was used to model the tension stiffening of reinforced concrete.

$$\sigma_t = \sigma_{cr}\left(\frac{\varepsilon_{cr}}{\varepsilon_t}\right)^n \quad ; \quad \varepsilon_{cr} = \frac{\sigma_{cr}}{E_0} \qquad (1)$$

Where: σ_t and ε_t tensile stress and strain in cracked concrete, respectively, σ_{cr} and ε_{cr} are concrete cracking tensile strength and cracking strain, respectively, E_0 is the concrete elastic modulus, and *n* is a number depending on the bond characteristic: 1/3 was proposed for the *n* value by Okamura and Maekawa [7], then Tamai et al. [8] used 0.4 for the deformed bar. Belarbi and Hsu [9] found that Eq.(1) was the best mathematical model to fit the descending branch of the tensile stress-strain curve with a power of 0.4. Moreover, An et al. [10] used the *n* value greater than 0.6 to model the tension softening based on fracture energy and the bond effect between steel and concrete. Kmiecik and Kaminski [11] proposed that for a given simulation, calibrate the *n* value with the predicted analysis results. Dere and Koroglu [12] proposed a simple relation of $0.7 + 1000\varepsilon_t$ to estimate the *n* value.

The above review for *n* value is related to the tension stiffening of concrete when reinforced with steel bars. Therefore, in this study, Okamura and Maekawa's [7] model was modified based on the experimental results to include the effect of BMF on the tension stiffening of concrete reinforced with BFRP bars as described below:

For concrete without BMF reinforced with BFRP bars, Eq. (2) was used to evaluate the n value.

$$n = 0.85 - \varepsilon_t \qquad (2)$$

whlie for concrete containing BMF and reinforced with BFRP bars, Eq.(3) was used to evaluate the *n* value. The contribution of BMF increases the tension stiffening of concrete, arresting the development of the crack because of the fiber bridging effect.

$$n = \left(0.85 - 10V_f\right) - {\varepsilon_t}^{3/4} \quad (3)$$

Where;V_f is the volume fraction of BMF

Figure 1 shows the tension stress-strain curves for each class of concrete used in this study. The ascending part of the curve is the tension resistance of concrete up to cracks appearing. And the curve descending part represents the tension stiffening of concrete due to reinforcing with BFRP bars and the contribution of BMF.

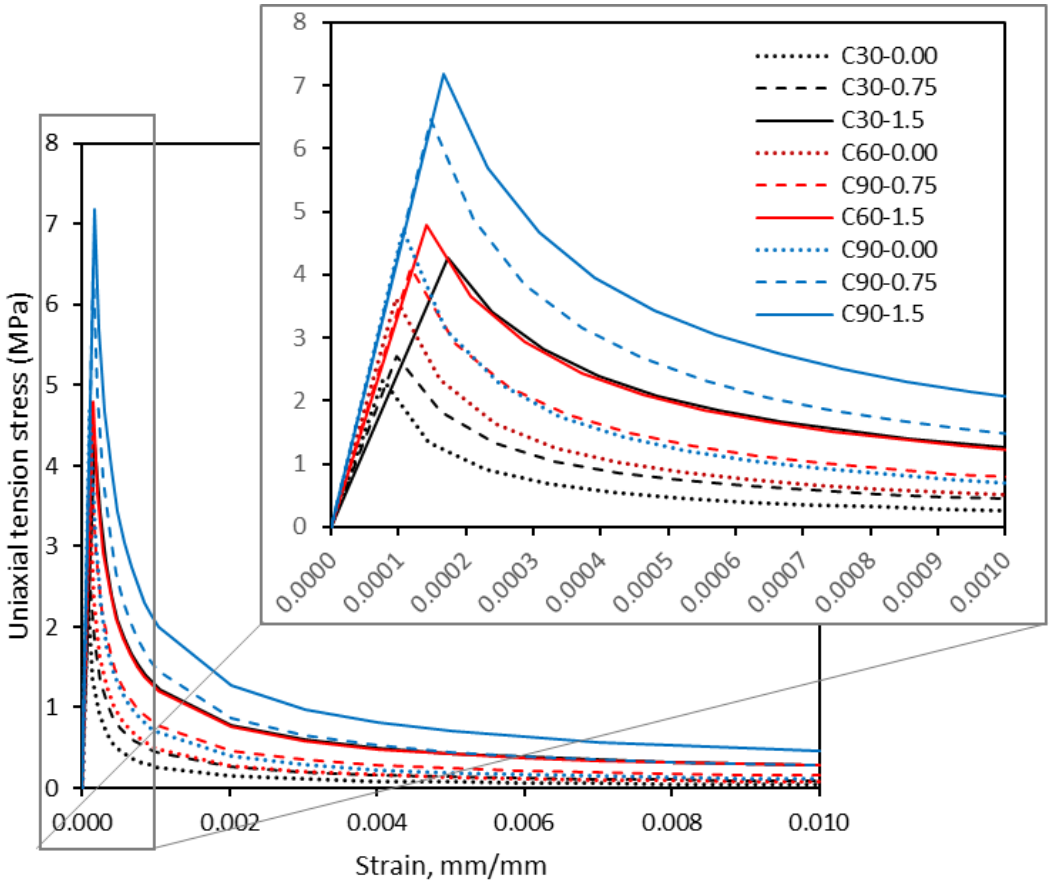

Figure 1 Tension stress-strain curves of various reinforced concrete

Generally, in reinforced concrete behavior, post-cracking is defined as the post-cracking stress as a function of cracking strain (ε_t^{ck}) as shown in **Figure 1**-a. The cracking strain is computed by subtracting the undamaged concrete's elastic strain (ε_{0t}^{el}) from the total strain (ε_t) as shown in Eq.(4) [6].

$$\varepsilon_t^{ck} = \varepsilon_t - \varepsilon_{0t}^{el} \quad , \qquad \varepsilon_{0t}^{el} = \frac{\sigma_t}{E_0} \tag{4}$$

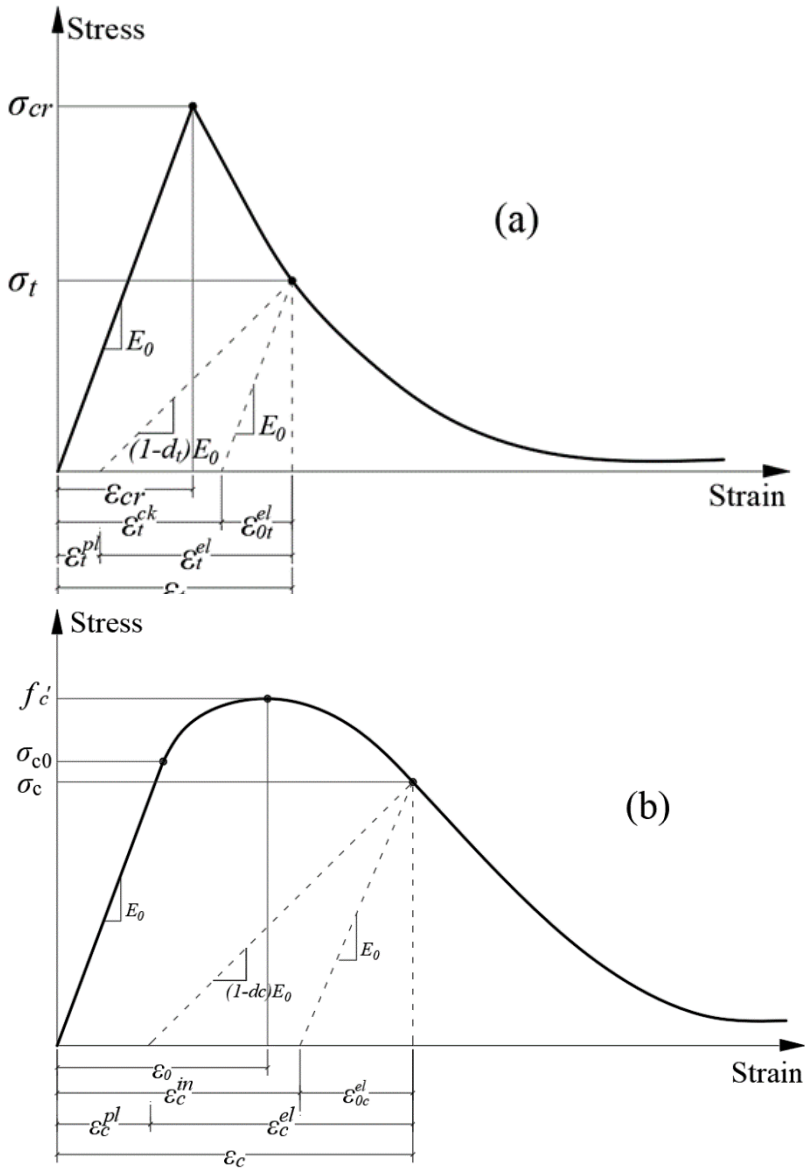

Figure 2 a) Definition of cracking strain and effect of damage on the elastic stiffness of concrete under tensile stress b) definition of inelastic strain and effect of damage on the elastic stiffness of concrete under compressive stress

1.1.2.2 Uniaxial compression stress behavior

The stress-strain behavior of uniaxial compression is a linear elastic relationship $\sigma_c = E_0\varepsilon_c$until the initial yield point. After that, the behavior

typically shows stress hardening followed by strain-softening beyond the ultimate stress in the plastic zone. Yang et al. [13] proposed a model as Eq. (5) to simulate the compressive stress-strain relationship of concrete. The suggested model estimates the stress-strain curve depending on concrete compressive strength and density. On the other hand, the ascending part of the curve well coincides with the experimental stress-strain curve. Therefore, this model was used to predict the compressive stress-strain curve of the concrete for each concrete class, as shown in Figure 3.

$$\sigma_c = f_c' \left[\frac{(\beta_1 + 1)\left(\frac{\varepsilon_c}{\varepsilon_0}\right)}{\left(\frac{\varepsilon_c}{\varepsilon_0}\right)^{\beta_1 + 1} + \beta_1} \right] \qquad (5)$$

Where:

$\beta_1 = 0.2e^{0.73\xi} \qquad for\ \varepsilon_c \leq \varepsilon_0$

$\beta_1 = 0.41e^{0.77\xi} \qquad for\ \varepsilon_c > \varepsilon_0$

$\varepsilon_0 = 0.0016e^{240(f_c'/E_0)}$

$\xi = (f_c'/f_0)^{0.67}(w_0/w_c)^{1.17}$

$f_0 = 10\ MPa$, refers to the concrete compressive strength reference value.

f_c' is the compressive strength of concrete

$w_0 = 2300\ kg/m^3$ is a reference value for the concrete density.

w_c is the concrete density.

The relation of the stress-strain curve beyond linear response is the inelastic relation between compressive stress and inelastic strain (ε_c^{in}). The compressive inelastic strain is obtained by subtracting the undamaged concrete's elastic strain. (ε_{0c}^{el}) from the total strain (ε_c) as shown in Eq.(6)

$$\varepsilon_c^{in} = \varepsilon_c - \varepsilon_{0t}^{in} \ , \qquad \varepsilon_{0t}^{in} = \frac{\sigma_c}{E_0} \qquad (6)$$

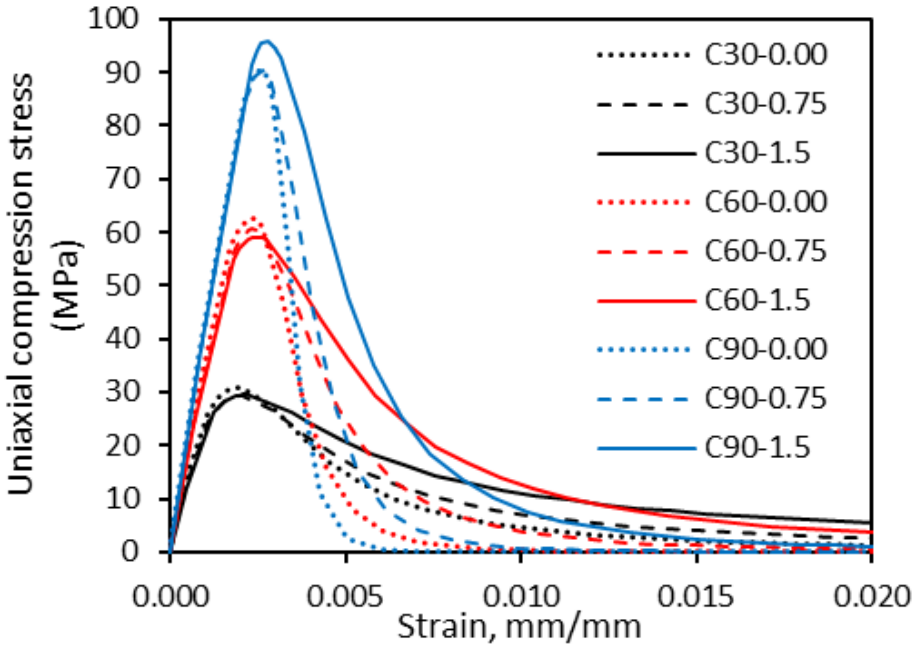

Figure 3 Compression stress-strain curves of various concrete class

1.1.3 Damage parameters

As shown in Figure 2-b, suppose the concrete sample is unloaded at any point from the strain-softening part of the stress-strain curves. In this case, a weakened unloading response is exhibited: the concrete elastic stiffness seems to be damaged or degraded. The damage to the elastic stiffness is represented by two damage factors, d_t, and d_c. Lubliner et al.[2] derived a simple model for plastic degradation of concrete, assuming that plastic degradation only occurs in the softening range and the stiffness is proportional to the cohesion. Based on this assumption, under uniaxial tension and uniaxial compression, the damage factors d_t and d_c are estimated from the following relationships, Eq(7) and Eq. (8)

$$d_t = 1 - \frac{\sigma_t}{\sigma_{cr}} \qquad (7)$$

$$d_c = 1 - \frac{\sigma_c}{f_c'} \qquad (8)$$

The damage variables range from zero, representing the undamaged material, to one, total strength loss. The damage parameters data were introduced to Abaqus in terms of damage factors, cracked strains, and inelastic strains. These damage factors reduce the elastic stiffness of the concrete in both tension and compression behavior, as illustrated in Figure 2. Abaqus changes the cracked strain and inelastic strain to plastic strain using these relationships, Eq. (9) and Eq. (10)

$$\varepsilon_t^{pl} = \varepsilon_t^{ck} - \frac{d_t\,\sigma_t}{(1-d_t)E_0} \qquad (9)$$

$$\varepsilon_c^{pl} = \varepsilon_c^{in} - \frac{d_c\,\sigma_c}{(1-d_c)E_0} \qquad (10)$$

1.1.3.1 Plasticity data

The dilation angle (ψ) is one of the main parameters required in Abaqus to be used in the plastic potential flow non-association rule. It is a volume change resulting from the shear distortion of an element in material and measured in the p-q plane. Vermeer and Borst [14] recommended a 13° for the dilation angle of concrete. Oñate et al. [15] used 32° as a dilation angle to analyze their models: plain cantilever concrete beam, prestressed cantilever beam, and simple tension model. At the same time, Lubliner et al. [2] to verification Concrete Damaged Plasticity Model (CDPM)) used a dilation angle of 15° in the model of the biaxial compression test proposed by Kupfer et al. [16]; this model had the uniaxial compression and tension strength of the concrete 32.8 MPa and 2.3 MPa, respectively. They used a dilation angle of 32° for the analysis of a notched beam that Arrea and Ingraffea [17] tested with the uniaxial compression and tension strength of the concrete 30 MPa and 2.75 MPa, respectively. Excellent agreement was observed between numerical results from Lubliner et al. [2] models with the experimental data from Kupfer et al. [16] and Arrea and Ingraffea [17]. In the same manner, Lee and Fenves [3] verified their model with the experimental biaxial compression test data of Kupfer et al. [16]; they used dilation angles 31° and 24° for the concrete. The result using 24° display good agreement with all

experimental data, whereas 31° yields a slightly different response. Jankowiak and Lodygowski [18] determined 38° based on a minimization of the error of the biaxial compression model of Kupfer et al.[16]. In a parameter study on a reinforced concrete beam loaded with two-point loads presented in Malm [19], for different dilation angles (10°, 20°, 30°, 40°, 50°, 56.3°), observed that the beam showed brittle behavior for small value of dilation angle and tended to ductile behavior with the higher value of dilation angle. Stoner and Polak [20] recommended for beams without stirrups a dilation angle of 30° but 50° for beams with stirrups. However, Abaqus's default value for the dilation angle is 15°.

It is evident from the above review that the value of the dilation angle changes in a wide range, and it must be calibrated with the experimental results. Therefore, in this study, the dilation angle after calibration was taken between 20° and 35°. Higher dilation angles were used for beams with better ductility because, as illustrated by Malm [19], the dilation angle of concrete is related to the ductility of members.

The Abaqus default values were used for other plasticity parameters; Flow potential eccentricity is $\epsilon = 0.1$, the ratio of initial biaxial compressive yield stress to initial uniaxial compressive yield stress is $\sigma_{b0}/\sigma_{c0} = 1.16$, the ratio of the second stress invariant on the tensile meridian to that on the compressive meridian at initial yield for any given value of the pressure invariant is $K_c = 0.667$

The elastic properties of concrete and elastic modulus and geometry of BFRP bars used in ABAQUS were obtained from experimental data.

1.2 Finite Element Results

The following sections compare the ABAQUS FEA results for all tested beams with the experimental data. The following comparisons were made: ultimate loads, load-deflection behavior, and crack patterns.

1.2.1 Load deflection curve

A comparison of experimental and FEA load-deflection curves for all beams is shown in Figure 4. The curves exhibit that the FEA with the experimental results coincided well over the whole range of behavior. All beams show identical pre-cracking, post-cracking, and ultimate load characteristics. Consequently, it has been demonstrated that ABAQUS can model BFRP-RC beams reinforced with BMF, both with and without stirrups. It can be observed that the FEA presented slight deviations in trends from the experimental trends in some beams, especially in the post-cracking stage. This might be due to some differences between FEA models and actual beams. In the FEA, the bonding between the concrete and BFRP bars was considered perfect (no slip), but in reality, little slip occurs. Furthermore, drying shrinkage causes microcracks. These might reduce the stiffness of the actual beams, but perfect homogeneous materials were assumed in the FEA simulation.

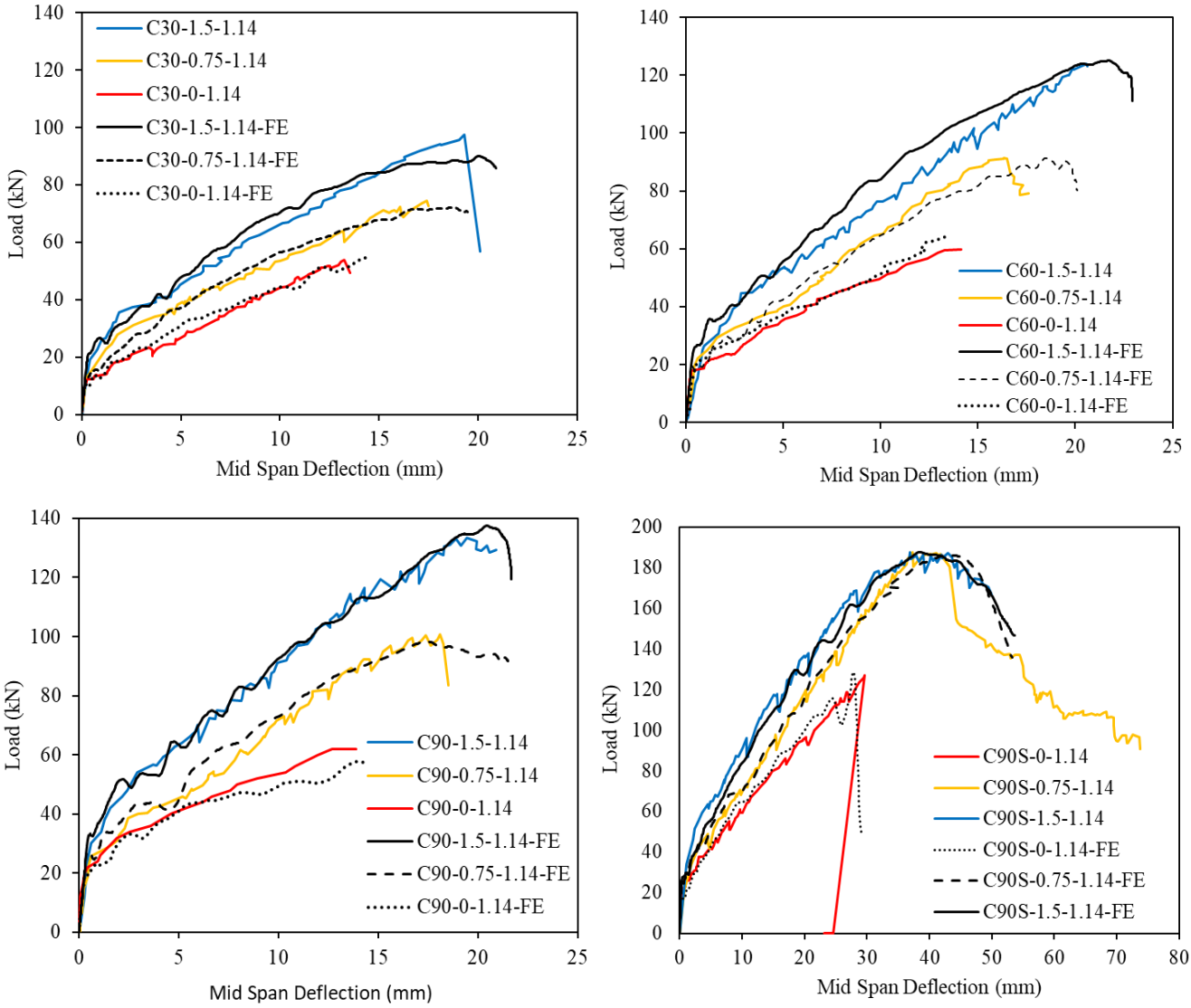

Figure 4 Effect of BMF on the load-deflection curve at mid-span of the tested beams and comparison with finite element analysis

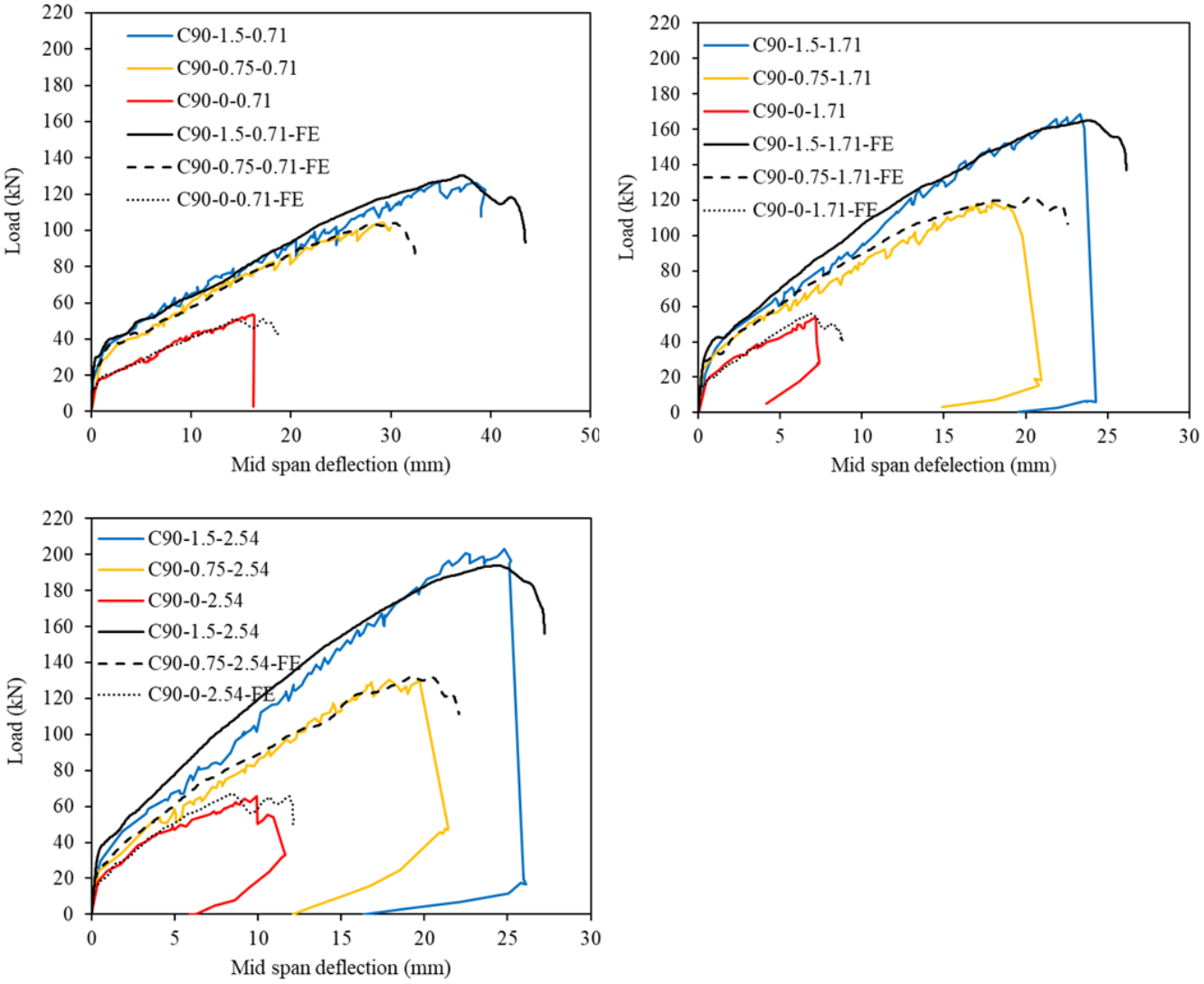

Figure 5 Effect of BMF on the load-deflection curve at mid-span of the tested beams and comparison with finite element analysis (continued)

1.2.2 Ultimate load

Table 1 and **Figure 6** show the comparison between experimental and analytical results of ultimate loads and mid-span deflection of the BFRP-BMF-RC beams. The comparisons are presented in the form of ultimate load $(P_{u,exp}/P_{u,FEA})$ and corresponding deflections at mid span $(\Delta_{u,exp}/\Delta_{u,FEA})$. The average ratios of $(P_{u,exp}/P_{u,FEA})$ and $(\Delta_{u,exp}/\Delta_{u,FEA})$ for the tested beams are 1.00 and 1.00 respectively. This shows that the FEA correctly evaluated the ultimate loads and deflections.

Table 1 Results of experimental and finite element analysis comparison of the beams

Beam Designations	EXP		FEA		$\frac{P_{u,exp}}{P_{u,FEA}}$	$\frac{\Delta_{u,exp}}{\Delta_{u,FEA}}$
	P_u (kN)	Δ_u (mm)	P_u (kN)	Δ_u (mm)		
C30-0-1.14	53.80	13.23	54.84	14.10	0.98	0.94
C30-0.75-1.14	74.41	17.41	72.16	18.70	1.03	0.93
C30-1.5-1.14	97.61	19.30	90.00	20.00	1.08	0.97
C60-0-1.14	59.76	14.13	64.17	13.33	0.93	1.06
C60-0.75-1.14	91.55	16.34	91.27	18.10	1.00	0.90
C60-1.5-1.14	123.85	20.58	124.99	21.74	0.99	0.95
C90-0-1.14	62.00	13.90	63.90	14.83	0.97	0.94
C90-0.75-1.14	100.42	18.11	98.32	17.37	1.02	1.04
C90-1.51.14	133.43	19.45	137.54	20.43	0.97	0.95
C90S-0-1.14	126.88	29.59	128.62	27.78	0.99	1.07
C90S-0.75-1.14	187.44	37.23	186.02	38.00	1.01	0.98
C90S-1.5-1.14	187.36	43.00	187.43	38.25	1.00	1.12
C90-0-0.71	53.57	16.12	51.08	14.47	1.05	1.11
C90-0.75-0.71	104.44	29.18	104.05	30.26	1.00	0.96
C90-1.5-0.71	126.5	34.87	130.29	37.05	0.97	0.94
C90-0-1.71	53.29	7.20	55.87	6.88	0.95	1.05
C90-0.75-1.71	118.82	17.93	121.60	20.38	0.98	0.88
C90-1.5-1.71	168.79	23.35	164.87	23.80	1.02	0.98
C90-0-2.52	65.62	9.93	66.90	8.34	0.98	1.19
C90-0.75-2.52	130.20	17.88	132.31	19.25	0.98	0.93
C90-1.50-2.52	203.32	24.81	193.79	24.43	1.05	1.02
				Mean	1.00	1.00
				SD	0.08	0.03

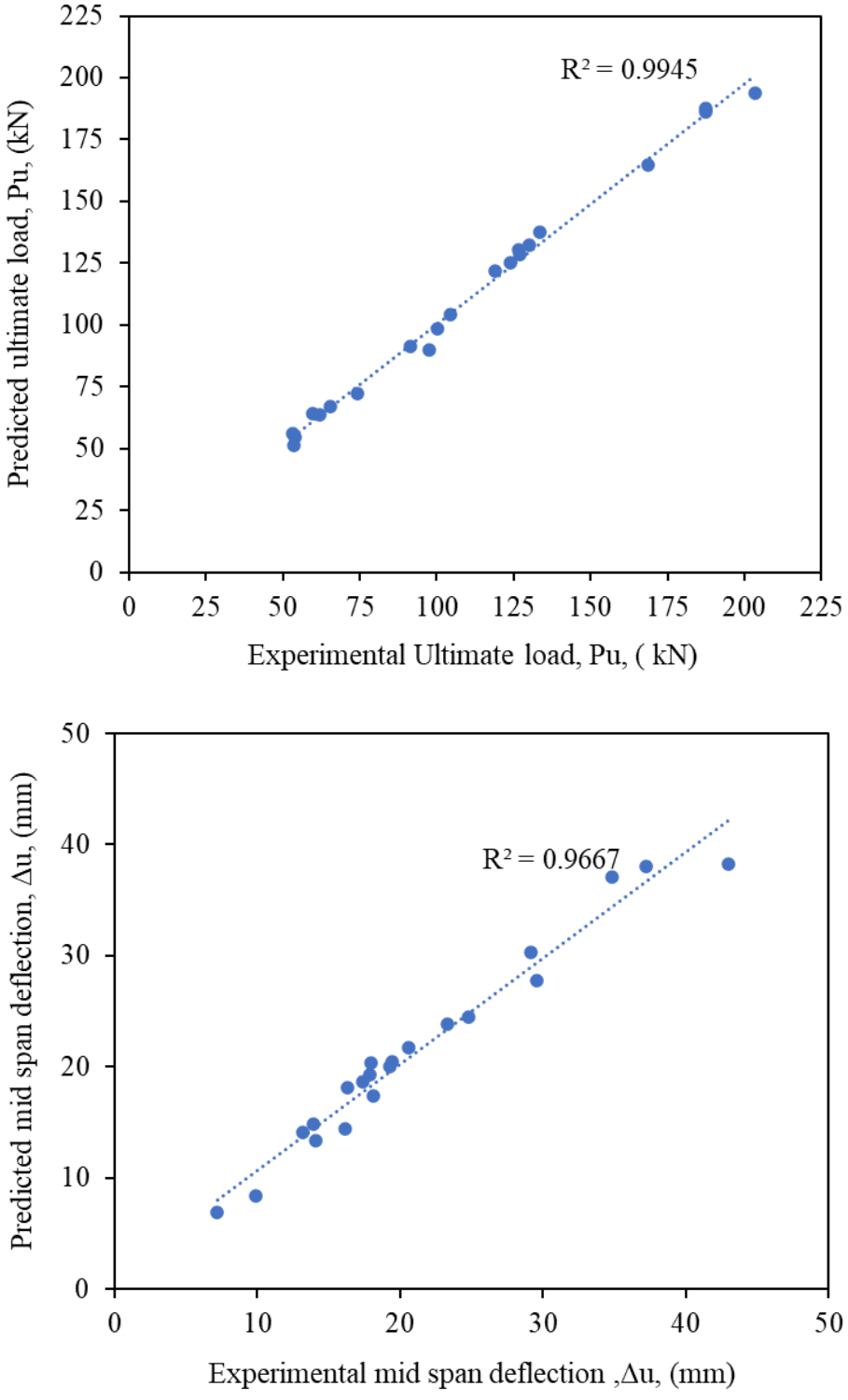

Figure 6 Comparison between experimental and FEA results at mid-span of Beams

1.2.3 Crack pattern

A tool for showing crack propagation at the concrete integration points or element centroid is not available in the ABAQUS FEA software. Other indicators, such as tensile damage, compressive damage, plastic strain, or logarithmic strain, might be considered indicators of crack formation.

Therefore, it was assumed in this study that the cracks started at the elements where tensile damage had occurred. **Figure 7** shows the tensile damage diagram from the FEA and the crack pattern from the experimental testing of the beams all tested beams. The red elements show that the element's tensile damage ratios are more than 90%. It can be seen that the outcomes of tensile damage of FEA and crack pattern of tested beams are largely comparable. It is clear that the number of cracks in beams that were reinforced with BMF is higher than those without BMF contribution because of the increasing tension stiffening of BFRP-RC beams due to the inclusion of BMF. And it is more remarkable in the HSC beams than NSC beams; for example, the number of cracks in beam C90-1.5-1.14 is higher than the number of cracks in compared counterpart beam C90-0-0.14.

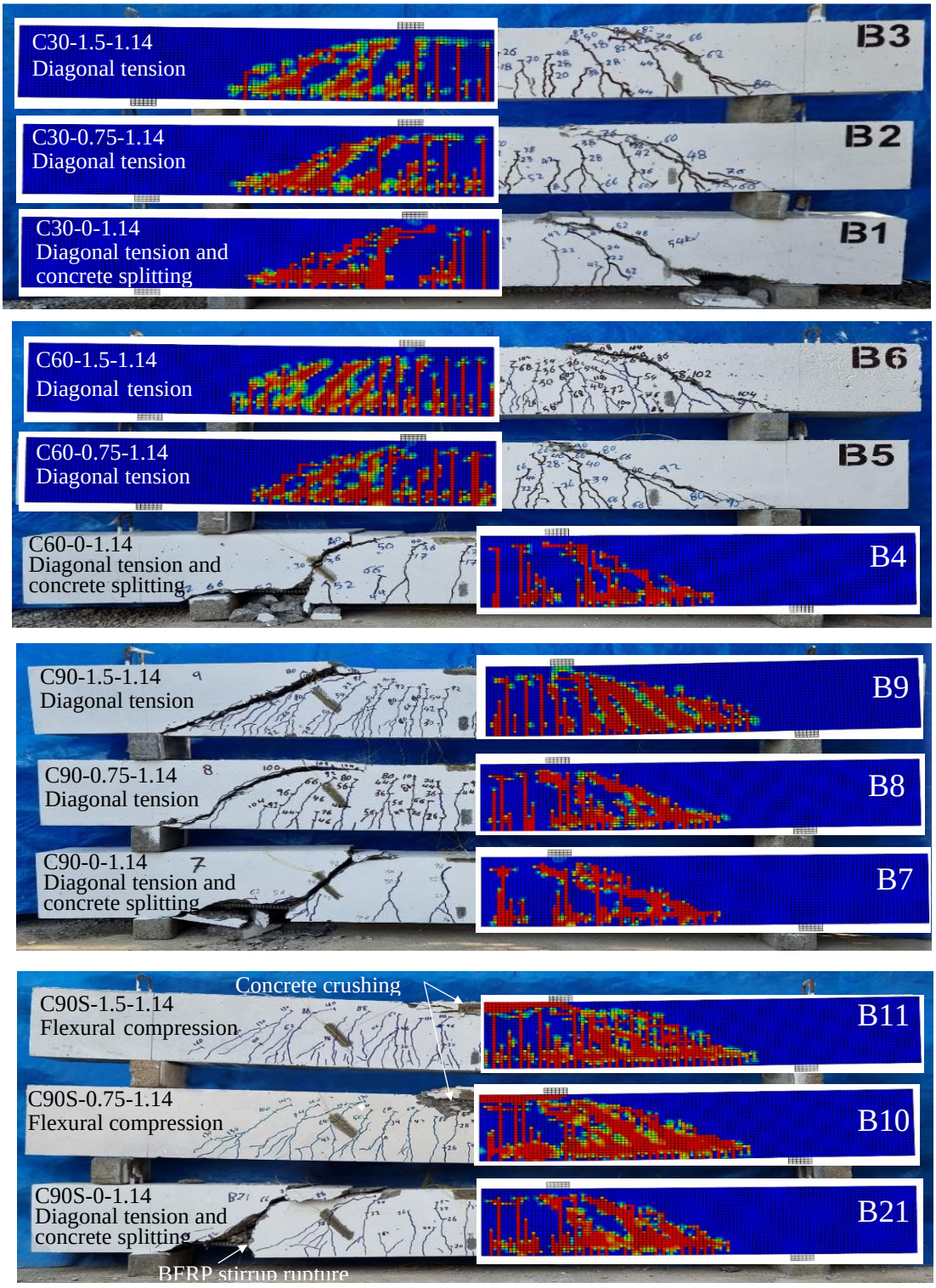

Figure 7 Comparison of the pattern of cracks in the tested beams and FEA

1.3 Conclusion

- It is acceptable to use the CDP model to predict the behavior of BFRP-RC beams reinforced with BMF with stirrups or not. The results of the FEA are in good agreement with those obtained by the experiments in terms of load-deflection behavior, failure mode, and crack pattern.
- The modified Okamura and Maekawa equation to predict the tension stiffening of RC showed an agreement result for all beams. It was modified based on the experimental data to include the effect of BMF on the behavior and capacity of BFRP-RC beams by considering the impact of BMF on the tension stiffening of concrete.

List of Abbreviations

BFRP: Basalt Fiber Reinforced Polymer

BMF: Basalt Macro Fiber

CDPM: Concrete Damage Plasticity Model

RC: Reinforced concrete

FEA: Finite Element Analysis

REFERENCES

[1] Dassault Systèmes, "GETTING STARTED WITH ABAQUS:INTERACTIVE EDITION." 3DS Dassault Systèmes, 2014.

[2] J. Lubliner, J. Oliver, S. Oller, and E. Onate, "A Plastic-Damage Model," *Int. J. Solids Struct.*, vol. 25, no. 3, pp. 299–326, 1989.

[3] J. Lee and G. L. Fenves, "Plastic-Damage Model for Cyclic Loading of Concrete Structures," *J. Eng. Mech.*, vol. 124, no. 8, pp. 892–900, 1998, doi: 10.1061/(asce)0733-9399(1998)124:8(892).

[4] J. J. Kim and M. Reda Taha, "Experimental and numerical evaluation of direct tension test for cylindrical concrete specimens," *Adv. Civ. Eng.*, vol. 2014, 2014, doi: 10.1155/2014/156926.

[5] A. P. Fantilli, H. Mihashi, and P. Vallini, "Multiple cracking and strain hardening in fiber-reinforced concrete under uniaxial tension," *Cem. Concr. Res.*, vol. 39, no. 12, pp. 1217–1229, 2009, doi: 10.1016/j.cemconres.2009.08.020.

[6] Dassault Systèmes, "ANALYSIS USER'S GUIDE VOLUME III: MATERIALS." 3DS Dassault Systèmes, 2014.

[7] H. Okamura, K. Maekawa, and S. Sivasubramaniyam, "Verification of modeling for reinforced concrete finite element," *Finite Elem. Anal. Reinf. Concr. Struct.*, no. May 1985, pp. 528–543, 1985.

[8] S. Tamai, H. Shima, J. Izumo, and H. Okamura, "Average stress-strain relationship in post yield range of steel bar in concrete," *Jsce*, vol. 6. pp. 117–129, 1987.

[9] A. Belarbi and T. T. C. Hsu, "Constitutive laws of concrete in tension and reinforcing bars stiffened by concrete," *ACI Struct. J.*, vol. 91, no. 4, pp. 465–474, 1994, doi: 10.14359/4154.

[10] X. An, K. Maekawa, and H. Okamura, "Numerical Simulation of Size Effect in Shear Strength of Rc Beams," *Doboku Gakkai Ronbunshu*, vol. 1997, no. 564, pp. 297–316, 1997, doi: 10.2208/jscej.1997.564_297.

[11] P. Kmiecik and M. Kamiński, "Modelling of reinforced concrete structures and composite structures with concrete strength degradation taken into consideration," *Arch. Civ. Mech. Eng.*, vol. 11, no. 3, pp. 623–636, 2011, doi: 10.1016/s1644-9665(12)60105-8.

[12] Y. Dere, "Nonlinear FE Modeling of Reinforced Concrete," *Int. J. Struct. Civ. Eng. Res.*, vol. 6, no. 1, pp. 71–74, 2017, doi: 10.18178/ijscer.6.1.71-74.

[13] K. H. Yang, J. H. Mun, M. S. Cho, and T. H. K. Kang, "Stress-strain model for various unconfined concretes in compression," *ACI Struct. J.*, vol. 111, no. 4, pp. 819–826, 2014, doi: 10.14359/51686631.

[14] P. A. Vermeer and R. de Borst, "Non-Associated Plasticity for Soils, Concrete and

Rock.," *Heron*, vol. 29, no. 3, pp. 1–64, 1984, doi: 10.1007/978-94-017-2653-5_10.

[15] E. Oñate, S. Olleri, J. Oliver, and J. Lubliner, "A constitutive model for cracking of concrete based on the incremental theory of plasticity," *Eng. Comput.*, vol. 5, no. 4, pp. 309–319, 1988, doi: 10.1108/eb023750.

[16] H. Kupfer, H. K. Hilsdorf, and H. Rusch, "Behavior of concrete under biaxial stresses," *ACI J.*, vol. 66, no. 8, pp. 656–666, 1969.

[17] M. Arrea, "Mixed-mode crack propagation in mortar and concrete," *Dept. Struct. Engrg. Rep.*, pp. 13–81, 1981.

[18] T. Jankowiak and T. Lodygowski, "Identification of parameters of concrete damage plasticity constitutive model," *Found. Civ. Environ. ...*, no. 6, pp. 53–69, 2005, [Online]. Available: http://www.ikb.poznan.pl/fcee/2005.06/full/fcee_2005-06_053-069_identification_of_parameters_of_concrete.pdf.

[19] R. Malm, "Shear cracks in concrete structures subjected to in-plane stresses," *Trita-Bkn. Bull.*, no. 88, p. 136p, 2006, [Online]. Available: http://www.diva-portal.org/diva/getDocument?urn_nbn_se_kth_diva-4215-2__fulltext.pdf%5Cnhttps://trid.trb.org/view/842709.

[20] J. G. Stoner and M. A. Polak, "Finite element modelling of GFRP reinforced concrete beams," *Comput. Concr.*, vol. 25, no. 4, pp. 369–382, 2020, doi: 10.12989/cac.2020.25.4.369.